Aalto University

OPEN ACCESS

This is an electronic reprint of the original article.
This reprint may differ from the original in pagination and typographic detail.

Nissi, Janita; Laakso, Ilkka

Magneto- and electrophosphene thresholds in the retina: a dosimetry modeling study

Published in:
Physics in Medicine and Biology

DOI:
10.1088/1361-6560/ac46df

Published: 07/01/2022

Document Version
Peer-reviewed accepted author manuscript, also known as Final accepted manuscript or Post-print

Published under the following license:
CC BY-NC-ND

Please cite the original version:
Nissi, J., & Laakso, I. (2022). Magneto- and electrophosphene thresholds in the retina: a dosimetry modeling study. *Physics in Medicine and Biology*, *67*(1), Article 015001. https://doi.org/10.1088/1361-6560/ac46df

This material is protected by copyright and other intellectual property rights, and duplication or sale of all or part of any of the repository collections is not permitted, except that material may be duplicated by you for your research use or educational purposes in electronic or print form. You must obtain permission for any other use. Electronic or print copies may not be offered, whether for sale or otherwise to anyone who is not an authorised user.

Magneto- and electrophosphene thresholds in the retina: a dosimetry modeling study

Janita Nissi[1] and Ilkka Laakso[1,2]

[1] Department of Electrical Engineering and Automation, Aalto University, Espoo, Finland
[2] Aalto Neuroimaging, Aalto University, Espoo, Finland

Abstract

Objective: Sensations of flickering light produced by time-varying magnetic fields or electric currents are called magneto- or electrophosphenes. Phosphene thresholds have been used in international guidelines and standards as an estimate of the thresholds of exposure that produce effects in the central nervous system. However, the estimated threshold values have a large range of uncertainty.
Approach: Phosphene thresholds were approximated by simulating five phosphene threshold experiments. Retinal electric fields and currents induced by electric and magnetic stimulation were calculated using the finite element method and 14 anatomically realistic computational models of human heads.
Main results: The radial component of retinal current density was determined to be in the range of 6.0 – 20.6 mA/m^2. This study produces more accurate estimates for threshold current density in the retina using detailed anatomical models and the estimates had a reduced range of uncertainty compared to earlier studies.
Significance: The results are useful for studying the mechanisms of retinal phosphenes and for the development of exposure limits for the central nervous system.

1 Introduction

Phosphenes are visual sensations caused by a stimulus other than light. When the stimulus is a time-varying magnetic field or an electric current, they are called magneto- or electrophosphenes. The sensations are often described as flickering lights and appear strongest at the peripheral parts of the visual field (Lövsund et al. 1980a, Kanai et al. 2008, Schutter and Hortensius 2010). Magneto- and electrophosphenes are suspected of resulting from low frequency fields interacting with the retina. Since the retina is considered a part of the central nervous system (CNS), phosphenes are regarded as one of the first signs of electric and magnetic fields interacting with the CNS (ICNIRP 2010). Consequently, in international guidelines and standards health and safety limits for low frequency (<400 Hz) field exposure are set to levels that protect against phosphenes (ICNIRP 2010, IEEE 2019). Though phosphenes themselves are transient and not considered adverse, there are unverified reports of CNS reactions, such as headaches and muscle spasms (IEEE 2019). Therefore, in the event that such effects occurred, then an exposure limit that protected against phosphenes should also protect against effects in the CNS.

Magnetic field exposure or currents applied directly to the head at various locations have been used experimentally to determine the ranges of source stimuli that exceed phosphene thresholds. However, if magneto- and electrophosphenes originate from the retina as hypothesized, it would be more accurate to determine the in situ stimulus dose that affects retinal tissue. However, there is no simple way to measure the current or electric field directly in a real retina. Instead, magneto- and electrophosphene threshold doses in the retina have been approximated using computational methods (Taki et al. 2003, Dimbylow 2011, Laakso and Hirata 2012a, 2013). Still, there is a large range of uncertainty in these threshold values (ICNIRP 2020, Wood 2008).

Both magneto- and electrophosphenes are induced at frequencies below 90 Hz, with stimulus threshold a function of frequency and the minimum threshold near 20 Hz. Since phosphene perception is prolonged by eye movement and abolished by applying pressure on the eyeball, phosphenes are suspected to originate from the electrical stimulation of the retina (Barlow et al. 1947, Brindley 1955) and the suggested stimulated retinal neurons include photoreceptors, bipolar and ganglion cells (Brindley 1955, Attwell 2003, Wood 2008). Phosphenes have also been reliably produced by applying alternating current through bipolar electrodes attached directly on the anaesthetized conjunctiva (Brindley 1955), which supports the hypothesis of retinal origin.

An alternative hypothesis suggests that electrical stimulation over the visual cortex, especially with transcranial alternating current stimulation (tACS), modulates the ongoing cortical activity directly under the stimulating electrode and influences phosphene perception (Kanai et al. 2008). This was challenged by another theory that phosphenes produced by occipital stimulation were caused by volume conduction from the occipital electrode to the retina (Schwiedrzik 2009). Experimental studies reported that phosphene thresholds increased when the stimulating electrode was moved away from the eye (Schutter and Hortensius 2010) and that there was no difference in the time it takes to evoke phosphenes with stimulation either near the eye or in the visual cortex (Kar and Krekelberg 2012). The spread of current from the occipital lobe to the retina has also been verified with computational modeling, reporting that a significant portion of the current flows through the retina and that the radial current density within the eye was estimated strong enough to elicit phosphenes (Laakso and Hirata 2012a, 2013).

Recently, Evans et al. (2021) suggested that even though cortical stimulation might not directly produce phosphenes in the visual cortex, it might contribute to the perception of phosphenes. In their study they confirmed that phosphene thresholds were lower for electrode montages that included a frontal electrode near the eyes. More importantly, they discovered that the thresholds differed between montages with the stimulating electrode placed near the frontal lobe (Fpz) and the reference located either at the vertex (Cz) or the occipital lobe (Oz). As the thresholds were lower for the Fpz-Oz montage than the Fpz-Cz montage, they suggested that stimulation of the visual cortex might facilitate phosphene perception. Similar effects have been reported by studies which combined transcranial magnetic and current stimulation (Antal et al. 2003, Kanai et al. 2010).

In this work, the exposure scenarios of different phosphene threshold experiments were investigated computationally with the aim of accurately characterizing the retinal threshold for magneto- and electrophosphenes and to reduce uncertainty in their values. The magnitude of current density and electric field intensity on the surface of the retina were calculated with an algorithm based on the finite element method and anatomically realistic models of human heads. Compared to earlier studies with only a few different anatomical models, the thresholds were calculated using fourteen unique models with a higher resolution and more detailed representation of the eye. The estimated threshold electric fields in the retina were also compared to the exposure limits set by the International Commission on Non-Ionizing Radiation Protection (ICNIRP) and the International Committee on Electromagnetic Safety of the Institute for Electrical and Electronic Engineers

(IEEE-ICES).

2 Methods and materials

2.1 Examined exposure scenarios

Phosphene thresholds were investigated by replicating the exposure conditions of individual studies published in the literature. To compare results among studies, the average thresholds at 20 Hz were used.

The first replicated experiment was a magnetophosphene study by Lövsund et al. (1980b), where a time-varying magnetic field was produced by a U-shaped electromagnet with its poles placed on the volunteers' temples. In this work, the magnetic field was generated with two magnetic point dipoles located near the temples of the model. To ensure the magnetic flux density inside the head was similar to the experiments of Lövsund et al., the dipoles were separated from the surface of the computational head model by 5 cm. The magnetic flux density measured near the eye, 2 cm from the temple, was set to 10 mT (rms) corresponding to the phosphene threshold reported at 20 Hz (background luminance 1.2 cd/m^2). Retinal threshold values were additionally calculated with magnetic flux density of 8.14 mT (rms, background luminance 3 cd/m^2). This value is from an article by Lövsund et al. (1979) and has been used by the International Committee on Electromagnetic Safety of the Institute for Electrical and Electronic Engineers (IEEE-ICES) to derive exposure reference limits for environmental magnetic fields (IEEE 2019).

The other experiments selected included the electrophosphene studies by Kanai et al. (2008), Kar and Krekelberg (2012) and Evans et al. (2019, 2021). Kanai et al. examined electrophoshenes induced by the Oz–Cz electrode montage according to the international 10-20 EEG system, while Kar and Krekelberg considered the Oz-Cz, Fpz-Cz and T5-Cz montages. Two studies of Evans et al. with slightly different thresholds were investigated. The first examined phosphenes with the Fpz-Cz and Oz-Cz montages (Evans et al. 2019) while the second also included the Fpz-Oz and T3-T4 montages (Evans et al. 2021). The montages are shown in Figure 1.

The thresholds were either assumed to be peak values of sinusoidal alternating current or were converted to peak from peak-to-peak values. In simulations, electric current was applied with sponge-type electrodes with a surface area matching that of the simulated experiment. A singular electrode consisted of a 6 mm thick, saline-saturated sponge, in the middle of which was a 1 mm thick rubber sheet. A connector disc was located in the middle

of the rubber and contained uniformly distributed current point sources or sinks.

2.2 Volume conductor models of head and eyes

Electric fields induced by magnetic and electric stimulation were investigated inside anatomically realistic, tissue segmented volume conductor models of human heads. The model resolution was 0.5 mm $\times$ 0.5 mm $\times$ 0.5 mm and each cubical voxel was assigned a discrete conductivity value depending on the tissue inside it. Fourteen individual models were created according to T1- and T2-weighted MR images of volunteers (Soldati and Laakso 2020).

An automatic algorithm was used to replace the tissue-segmented eyes with ones consisting of separate tissue layers for sclera, cornea, retina, lens and vitreous humor (Figure 2). The outermost voxel layers were divided between the sclera and the cornea. The sclera consisted of the surface of the eyeball within 150 degrees from the posterior pole using the center of the eye as the origin. The thickness of the sclera decreased linearly from 1 mm in the posterior pole to 0.5 mm near the edge. The remaining anterior surface consisted of the cornea and its thickness ranged from 0.5 mm in the center to 1 mm in the periphery. The retina was modeled underneath the sclera as a 0.5 mm thick layer and covered the area within 135 degrees from the posterior pole. The thicknesses of the ocular tissue layers were based on published values (Vurgese et al. 2012, Artal 2017). The size and location of the lens were obtained from the MR images (Figure 3) by simple thresholding followed by smoothing of its surface. The rest of the voxels inside the eye were included into the vitreous humor. The optic nerve was also detected from the MR images with thresholding and modeled as a homogeneous segment behind the eye, within 10 mm radius from the sclera. In the grid composed of 0.5 mm cubical voxels, each voxel of the eyes used the average conductivity of the tissues inside it as can be seen in Figure 4.

2.3 Electrical conductivity of tissues

The conductivities of biological tissues (Table 1) were assumed to be homogeneous and isotropic. The skull was composed of cortical and cancellous bone for which the conductivities were obtained from Akhtari et al. (2002) and increased by 25% to account for the difference between room and body temperature. The mucous membrane was assigned the same conductivity as cortical bone to prevent current flow through the nasal cavity. The conductivity of the gray matter was assigned the average of multiple values (Akhtari

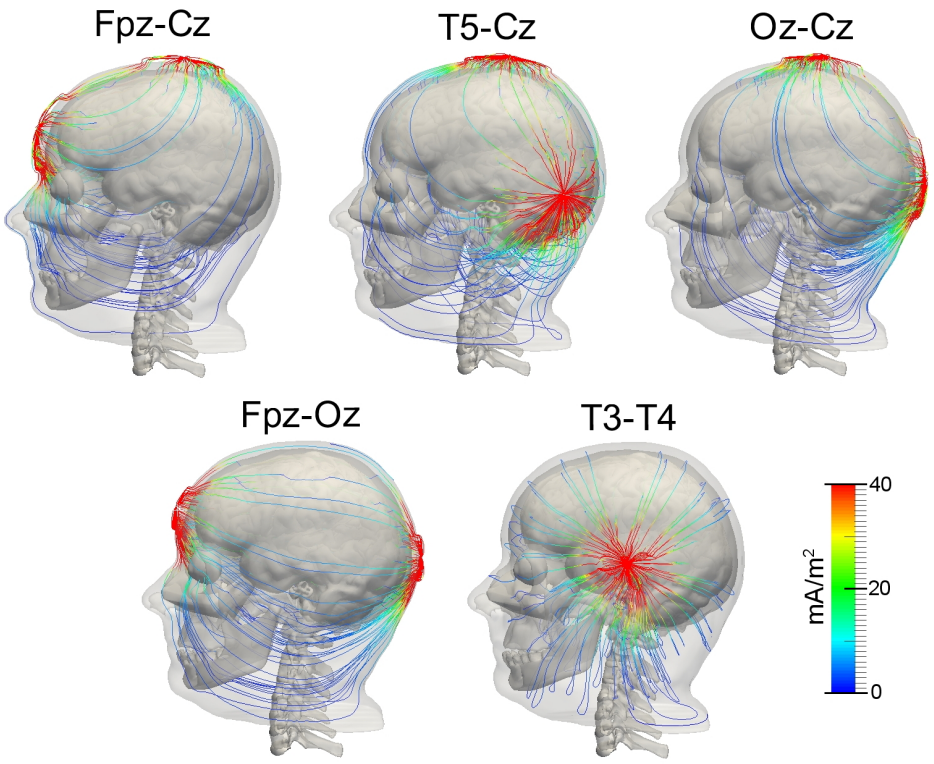

Figure 1: Current flow between electrodes in each electrical exposure scenario.

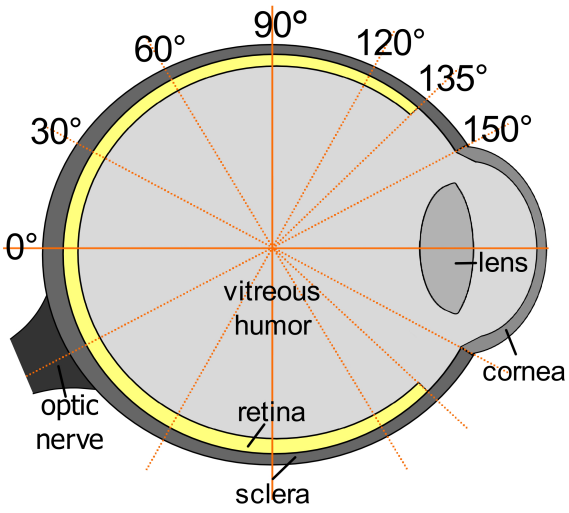

Figure 2: Graphical representation of the tissue layers inside the eye model. Angles are measured from the posterior pole (0°) using the center of the eyeball as the origin.

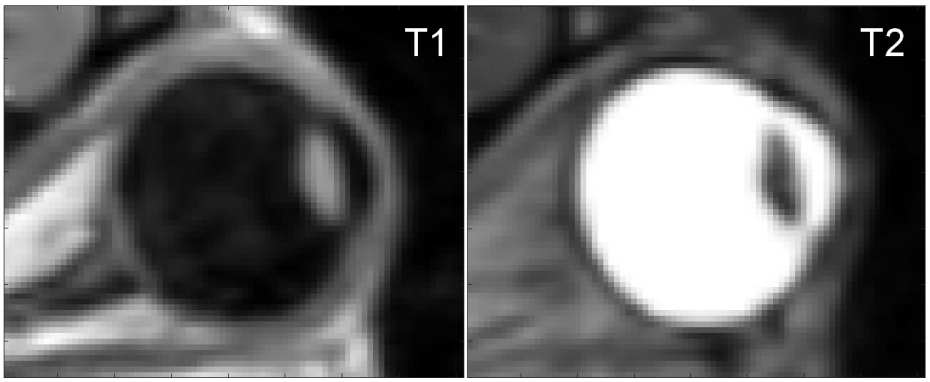

Figure 3: T1 and T2 weighted MR images of the eye.

et al. 2006, Latikka et al. 2001, Gabriel et al. 1996a) and white matter conductivity was adjusted to 70% of gray matter (Gabriel et al. 1996a). The optic nerve was assigned the same value as the white matter. The conductivity of cerebrospinal fluid was taken from Baumann et al. (1997) and blood conductivity from Gabriel et al. (1996a). Scalp conductivity was from McCann et al. (2019). Due to the difficulty segmenting between muscle and fat, both were blended together using a weighted average with 2/3 weight to muscle (Gabriel et al. 1996a, McCann et al. 2019) and 1/3 weight to fat (Gabriel et al. 1996b, 2009). The conductivities of the sclera, cornea, lens and vitreous humor were obtained from Lindenblatt and Silny (2001). Though Lindenblatt and Silny did not measure the conductivity of the retina, they deduced that it should have a value similar to that of the vitreous humor. On the other hand, Wood (2008) argued that due to the thinness of the retinal layer it should use the same value as the sclera. In this work, the conductivity of the retina is the same as blood, as it falls between these two estimates. Although the conductivities of the retina and other ocular tissues were assumed to be homogeneous throughout the eye, experimental evidence suggests that the conductivities might vary radially (Brindley 1956). The remaining tissue conductivities were inferred from the aforementioned values.

2.4 Determination of electric field

The electric field was determined under quasi-static assumption by solving the electric scalar potential equation (Wang and Eisenberg 1994) for magnetic stimulation

$$\nabla \cdot \sigma \nabla \phi = -\nabla \cdot \sigma \frac{\partial \mathbf{A}}{\partial t} \tag{1}$$

and for electric stimulation

$$\nabla \cdot \sigma \nabla \phi = -\frac{\partial \rho_s}{\partial t}. \tag{2}$$

Here ϕ is the electric scalar potential, σ is the electrical conductivity, $\mathbf{A}$ is the magnetic vector potential and $\frac{\partial \rho_s}{\partial t}$ is the source/sink of the electric current. The normal component of the current density at body surface is assumed to be zero ($\mathbf{n} \cdot \mathbf{J} = 0$).

In this work, the scalar potential equation was solved numerically with an in-house solver based on the finite element method (FEM) with piece-wise linear basis functions (Laakso and Hirata 2012b). The head models were discretized into a uniform grid of cubical voxels with a side length of 0.5 mm and the system of linear equations was iteratively solved until the relative

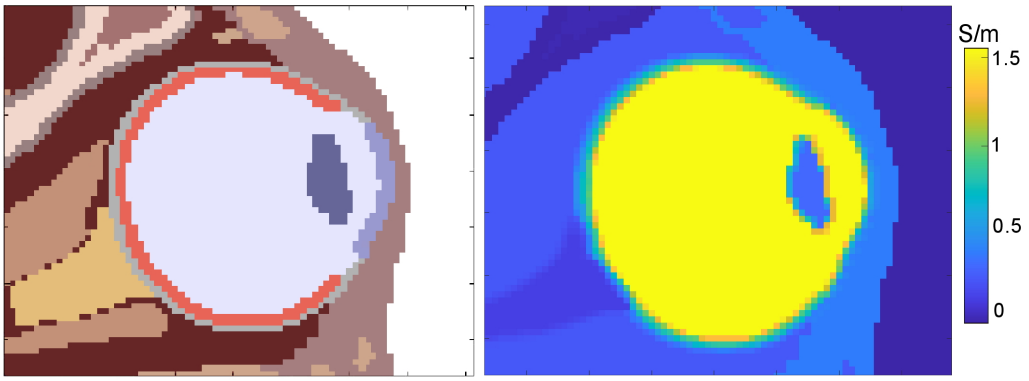

Figure 4: (Left) Voxelized eye after segmentation. (Right) Conductivity of the ocular tissues in a grid of cubical voxels.

Table 1: The electrical conductivities of tissues collected from literature data.

Tissue	**(S/m)**		**Tissue**	**(S/m)**	
Blood	0.7	(Gabriel et al. 1996a)	Glands	0.5	
Bone (Cancellous)	0.027*	(Akhtari et al. 2002)	Muscle	0.35	(Gabriel et al. 1996a, McCann et al. 2019)
Bone (Cortical)	0.008*	(Akhtari et al. 2002)	Lens	0.32	(Lindenblatt Silny 2001)
Brain (Gray matter)	0.2	(Akhtari et al. 2006, Latikka et al. 2001, Gabriel et al. 1996a)	Scalp	0.4	(McCann et al. 2019)
Brain (White matter)	0.14		Sclera	0.56	(Lindenblatt Silny 2001)
Cartilage	0.18		Spinal cord	0.03	
Cerebellum	0.2		Tendon	0.3	
Cerebrospinal fluid	1.8	(Baumann et al. 1997)	Trachea	0.3	
Cornea	0.5	(Lindenblatt Silny 2001)	Vitreous humor	1.55	(Lindenblatt Silny 2001)
Fat	0.08	(Gabriel et al. 1996b, 2009)	Retina	0.7	

* Increased by 25 % to compensate for room temperature measurements.

residual norm was below 10^{-6}. The electric field was then calculated from the gradient of the scalar potential ($\mathbf{A} = 0$ for electric stimulation):

$$\mathbf{E} = -\nabla\phi - \frac{\partial \mathbf{A}}{\partial t}. \tag{3}$$

2.5 Analysis of the current density in the retina

Phosphene thresholds in the retina were investigated with respect to the magnitude of the current density (peak values). Assuming phosphenes originate from the retina and the sensitivity to electrical stimulation across the retina is uniform, phosphenes are produced when the maximum current density or electric field intensity exceeds an unknown threshold. Here, the 99th percentile values of dose were used instead of the maximum value to reduce numerical error in the estimated retinal thresholds. The values were first determined separately for all anatomical models and then the averages were calculated for the entire group. Similarly, to determine the average distribution of current density, the retina was converted to spherical coordinates and current density was calculated at the same coordinate points on all models. As the coordinates were the same, the current density values could be averaged across the whole group and used to create the images of the average distribution on the retina. Additionally, the intensity of the threshold electric field in the retina was calculated by dividing the 99th percentile current density with a constant conductivity value of 0.7 S/m and scaling from peak to root mean square (rms) values.

3 Results

3.1 Current density distribution in the retina

The average distributions of radial current density on the retina for all stimulation scenarios are shown in Figure 5. The magnetic stimulation used flux density of 10 mT and electrical stimulation scenarios used 100 µA current. The distributions of the left and right eye were symmetrical in all examined cases, though the current density in the left eye for the T5-Cz montage was slightly higher. The maximum radial current density for magnetic stimulation, T5-Cz and Oz-Cz montages was located on the inferior side of the orbit and a secondary maximum was on the superior side. Both primary

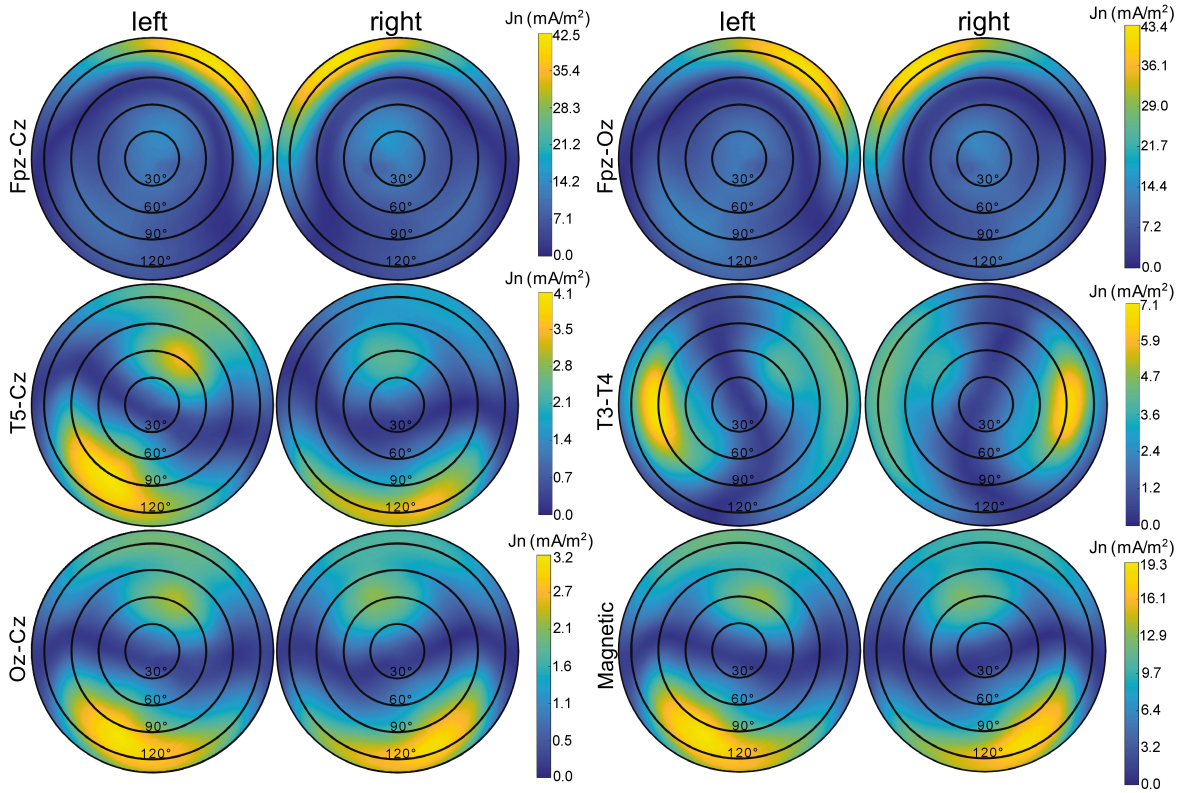

Figure 5: Average distribution of radial current density ($\mathbf{J}_n$, peak value) across the left and right retina (0°– 135°) induced by magnetic (10 mT, rms) or electric (100 µA, peak) stimulation. The black circles denote the angle from posterior pole of the orbit every 30 degrees (Figure 2).

Table 2: Magnitude of the (99th percentile) threshold current density ($\mathbf{J}$) and its radial component ($\mathbf{J}_n$) on the retina within 135 and 90 degrees from the posterior pole of the eyeball. Unless stated otherwise thresholds are given in µA (peak) and current densities in mA/m^2 (peak).

Scenario	**Source**	**Threshold**	**0 – 135 degrees**		**0 – 90 degrees**	
			J	**$\mathbf{J}_n$**	**J**	**$\mathbf{J}_n$**
Lövsund et al.	temples	10 mT (rms)	22.5 ± 2.1	19.3 ± 2.3	17.5 ± 2.6	16.2 ± 2.4
		8.14 mT (rms)	18.3 ± 1.7	15.7 ± 1.9	14.2 ± 2.1	13.2 ± 2.0
Kanai et al.	Oz-Cz	550	17.9 ± 2.4	17.3 ± 2.3	15.6 ± 2.2	14.9 ± 2.2
Kar &	Fpz-Cz	60	24.5 ± 5.9	23.9 ± 5.8	11.7 ± 2.9	8.8 ± 1.4
Krekelberg	T5-Cz	150	6.6 ± 0.8	6.4 ± 0.8	6.2 ± 0.9	6.0 ± 0.9
	Oz-Cz	230	7.6 ± 1.0	7.4 ± 1.0	6.7 ± 0.9	6.4 ± 1.0
Evans et al.	Fpz-Cz	150	59.0 ± 11.3	57.7 ± 11.1	28.7 ± 7.6	20.6 ± 3.3
(2019)	Oz-Cz	560	18.7 ± 2.5	17.4 ± 2.5	16.4 ± 2.3	15.7 ± 2.4
Evans et al.	Fpz-Oz	56.25	23.3 ± 4.5	22.7 ± 4.4	11.2 ± 3.0	8.0 ± 1.2
(2021)	Fpz-Cz	87.5	34.4 ± 6.6	33.7 ± 6.5	16.8 ± 4.4	12.0 ± 1.9
	T3-T4	143.75	10.2 ± 1.9	9.9 ± 1.8	9.7 ± 1.6	9.4 ± 1.6
	Oz-Cz	318.75	10.6 ± 1.5	9.9 ± 1.4	9.3 ± 1.3	8.9 ± 1.4

Table 3: Difference in the (99th percentile) radial current density on the retina caused by the displacement of an electrode. The first electrode was moved by 2 cm from its correct position in respect to the 10-20 system while the second electrode remained in its original position. Direction of the displacement was either toward the nasion (−) or the inion (+) following the mid-sagittal plane along the surface of the head.

Montage		**Direction**	**Difference (%)**	
Electrode 1	**Electrode 2**	**of displacement**	**$\mathbf{J}_n$ (0°– 135°)**	**$\mathbf{J}_n$ (0°– 90°)**
Fpz	Oz	+	−41	−30
Fpz	Cz	+	−44	−44
Oz	Fpz	−	−1.0	−0.9
Oz	Fpz	+	1.2	1.5
Cz	Fpz	−	−4.3	−2.7
Cz	Fpz	+	2.7	1.3
Oz	Cz	−	−22	−21
Oz	Cz	+	29	28
Cz	Oz	−	17	18
Cz	Oz	+	−16	−16

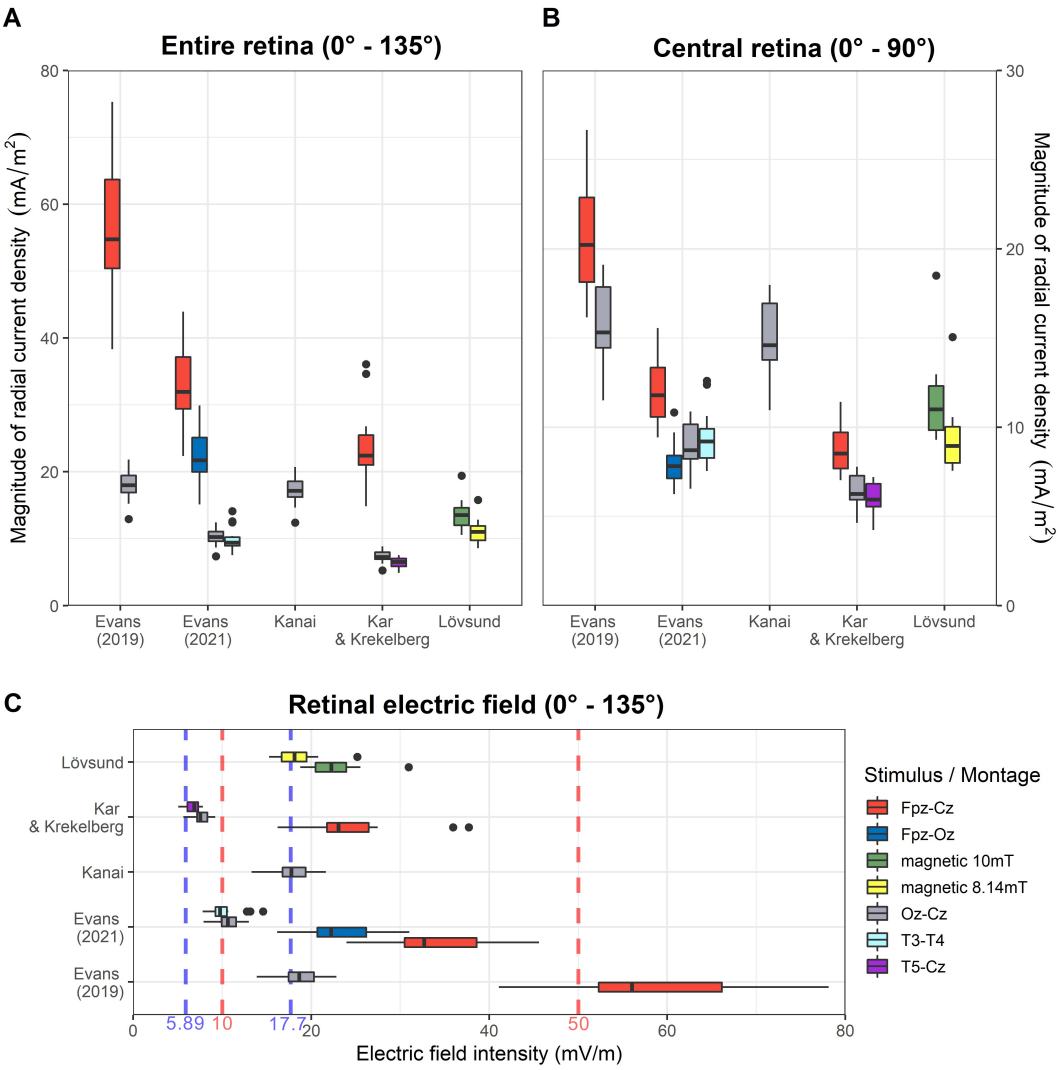

Figure 6: 99th percentile retinal thresholds of 14 unique models. (A) Magnitude of radial current density (peak) at phosphene threshold for the entire surface of the retina. (B) Magnitude of radial current density (peak) at phosphene threshold in the center of the retina within 90 degrees from the posterior pole. (C) Threshold electric fields (rms) calculated from current density with constant conductivity of 0.7 S/m. Electric field intensities were compared with the 20 Hz exposure limits specified by ICNIRP guidelines (2010) and IEEE-ICES standard (2019). The red dashed lines denote the ICNIRP exposure limits at 20 Hz for the general public (10 mV/m) and occupational exposure (50 mV/m), and blue dashed lines the IEEE-ICES restrictions for people in unrestricted (5.89 mV/m) and restricted environments (17.7 mV/m).

and secondary maxima were located within 120 degrees from the center of the retina. The maxima of the T3-T4 montage was located on both sides of the orbit, near 90 degrees from the posterior pole. The primary maximum was located on the left side of the left eye and on the right side of the right eye. The current distributions of Fpz-Cz and Fpz-Oz montages were nearly identical. The primary maximum was located on the superoanterior edge of the retina and a secondary maximum was found near the center.

3.2 Retinal current density at phosphene threshold

The total and radial current densities were then scaled to according to the threshold stimuli of the respective exposure scenarios. The average magnitudes of current density at phosphene threshold are presented in Table 2 for the entire retina (0°– 135°) and its central area (0°– 90°). Figures 6A and B show the variation in the retinal thresholds among the 14 models for each scenario. On the entire retina the magnitude of the radial current density (mean ± standard deviation, peak values) ranged from 6.4±0.8 to 57.7±11.1 mA/m^2 and the total current density from 6.6±0.8 to 59.0±11.3 mA/m^2. When only the central area of the retina was considered, the magnitude of the threshold radial and total current density varied less across all scenarios. The radial current density ranged from 6.0 ± 0.9 to 20.6 ± 3.3 mA/m^2 and the total current density from 6.2 ± 0.9 to 28.7 ± 7.6 mA/m^2.

The intensities of retinal electric fields (rms) at phosphene threshold were also calculated (Figure 6C) and compared to low frequency, electric and magnetic field exposure limits set by the ICNIRP and IEEE-ICES. All threshold electric field intensities were near or higher than the 20 Hz general public restrictions of ICNIRP (10 mV/m, rms) and IEEE-ICES (5.89 mV/m, rms). Considering the occupational exposure limits, the retinal electric field at phosphene threshold was higher than the ICNIRP limit (50 mV/m, rms) only for the Fpz-Cz montage of Evans et al. (2019) scenario. On the other hand, the intensity of the retinal electric field exceeded the respective IEEE-ICES limit (17.7 mV/m, rms) in all but four cases.

3.3 Effect of electrode displacement

The results are based on threshold data collected from the literature and though the exposure conditions were carefully replicated in the simulations, there could be differences between the electrode placement of this work and the experiments. Therefore, variations in the retinal current density caused by the displacement of electrodes were examined with three montages on the mid-sagittal plane. The selected montages were Fpz-Oz, Fpz-Cz and Oz-Cz.

The electrodes were displaced by 2 cm from their position in respect to the 10-20 system and only one electrode was moved at a time. The displacements followed the line between the nasion (the bridge of the nose) and inion (the highest point of the occipital bone protuberance) on the surface of the model. The effect on the 99th percentile radial current densities of the retina are listed in Table 3.

The displacement of the Fpz electrode had the greatest effect on the retinal current density with a decrease of over 30%. Moving the Oz and Cz electrodes had only minor effects when connected to the Fpz electrode but affected the current greatly in the Oz-Cz montage. The displacement of the Oz electrode either increased or decreased the current density by over 20% while the Cz electrode changed the value by approximately 17%. In general, moving the electrodes closer to each other decreased the current density in the retina while increasing the distance between electrodes had an opposite effect.

4 Discussion

Phosphene thresholds on the retina were calculated by simulating the exposure conditions of five experiments. In the current distributions of Oz-Cz and T5-Cz montages, the maximum current density was located in the peripheral retina. This agrees with experimental studies, where phosphenes were observed in the peripheral parts of the visual field (Kanai et al. 2008, Schutter and Hortensius 2010). Similarly, the maximum of the Lövsund et al. (1980b) scenario with a magnetic stimulus was located on the peripheral retina. Though Lövsund et al. did not report where in the visual field phosphenes were observed, other studies have stated that magnetophosphenes appear strongest in the periphery (Barlow et al. 1947, Taki et al. 2003). The montages that included the Fpz electrode had a primary maximum in the periphery and a secondary maximum near the center of the retina. This could be the reason why experimental studies that used the same montages reported both peripheral and central phosphenes (Schutter and Hortensius 2010, Evans et al. 2019). The distributions were similar to predictions made by Laakso and Hirata (2012a, 2013).

Since experimental studies suggest that the retina is more sensitive to stimulation from radial current (Brindley 1955), it should be appropriate to define retinal phosphene threshold in terms of radial current density. There are many proposed sites for phosphene generation in the retina, of which radial stimulation would affect radially oriented retinal cells (photoreceptors, bipolar and ganglion cells) rather than tangentially oriented cells (horizontal

and amacrine cells) (Attwell 2003). The magnitude of radial current density induced by threshold intensity stimulus was determined to be in the range of 6.4 – 57.7 mA/m^2 on the entire retina, and 6.0 – 20.6 mA/m^2 within 90 degrees from its center. Assuming also that the Fpz-Cz montage can in fact evoke phosphenes near the center of the visual field, the central current densities might provide a more accurate estimate of the threshold. For the central retina, the average magnitude of radial current density at phosphene threshold across all examined scenarios was roughly 12 mA/m^2. This result is similar to the estimations of other computational studies (Taki et al. 2003, Laakso and Hirata 2012a, 2013) and the estimate by Lövsund et al. based on magnetophosphene data (1980a). Notably, the range of variability in the central retina is considerably narrower than that of previous estimates (Wood, 2008).

In the study of Evans et al. (2021), electrophosphene thresholds were examined with four different montages. They found that thresholds were lower for the Fpz-Oz montage compared to the Fpz-Cz montage suggesting that stimulation of the occipital cortex influences phosphene perception. Similarly, scaling the retinal current densities according to respective thresholds resulted in slightly different retinal threshold values for the Fpz-Cz and Fpz-Oz. However, these thresholds were obtained using an alternating current with a DC offset, while the other studies had used alternating current stimulation without an offset.

The threshold electric field intensities in the retina were also calculated and compared with the exposure limits of IEEE-ICES and ICNIRP (ICNIRP 2010, IEEE 2019). The electric field thresholds mostly exceeded the IEEE-ICES 20 Hz exposure limit for restricted environments, but many were below the respective ICNIRP limit for occupational exposure. Since the calculated electric field intensities do not exceed the exposure limits depending on the examined scenario, phosphenes could be produced by fields weaker than previously estimated. However, as the threshold electric field was calculated from retinal current density, it depends greatly on the conductivity chosen for the retina and estimates include a large range of variation between 0.01 and 1.5 S/m (Attwell 2003, Wood 2008). Here, a conductivity of 0.7 S/m was used. The radial current density provides a more reliable estimate of the threshold than the electric field as it is only slightly affected by the chosen conductivity.

This study has some limitations. Firstly, the results were scaled according to literature data on magneto- and electrophosphene thresholds which varied significantly due to differences in experimental conditions between studies. Phosphene perception is also affected by a number of factors, such as environmental lighting (Kanai et al. 2008), dark-adaptation state of the eyes

(Lövsund et al. 1980b), blinking or eye movement (Adrian 1977, Barlow et al. 1947). Additionally, the studies used a different number of subjects, duration of the stimulus and even the definition of a phosphene threshold. Thus, comparing thresholds between separate experiments is not straightforward. Finally, the results indicated inter-individual variations in the retinal current densities and electric fields. The anatomical models used herein were not the same individuals who participated in the experiments, which could cause bias in the estimated threshold values.

5 Conclusion

Retinal phosphene thresholds were characterized in regard to magnitude of the current density and electric field intensity using realistic computational head models and an algorithm based on the finite element method. The radial current density corresponding to phosphene perception threshold in the retina was found to be in the range of 6.0 – 20.6 $\mathrm{mA/m^2}$. The results are based on a more detailed approximation of the human head compared to previous estimates and had reduced range of uncertainty. The results of this study provide more accurate estimates for the retinal current density at phosphene threshold for the development of electric and magnetic field exposure limits and the investigation of phosphene production in the retina.

Acknowledgements

This work was partially supported by the Academy of Finland under Grant 325326. The authors would like to thank Marco Soldati for the creating the original computational models.

References

Adrian, D. J. (1977). Auditory and visual sensations stimulated by low-frequency electric currents. *Radio Science*, 12(6S):243–250.

Akhtari, M., Bryant, H., Mamelak, A., Flynn, E., Heller, L., Shih, J., Mandelkem, M., Matlachov, A., Ranken, D., Best, E., et al. (2002). Conductivities of three-layer live human skull. *Brain topography*, 14(3):151–167.

Akhtari, M., Salamon, N., Duncan, R., Fried, I., and Mathern, G. (2006). Electrical conductivities of the freshly excised cerebral cortex in epilepsy surgery patients; correlation with pathology, seizure duration, and diffusion tensor imaging. *Brain Topography*, 18(4):281.

Antal, A., Kincses, T. Z., Nitsche, M. A., and Paulus, W. (2003). Manipulation of phosphene thresholds by transcranial direct current stimulation in man. *Experimental brain research*, 150(3):375–378.

Artal, P. (2017). *Handbook of Visual Optics, Volume I - Fundamentals and Eye Optics*. CRC Press.

Attwell, D. (2003). Interaction of low frequency electric fields with the nervous system: the retina as a model system. *Radiation protection dosimetry*, 106(4):341–348.

Barlow, H. B., Kohn, H. I., and Walsh, E. G. (1947). Visual sensations aroused by magnetic fields. *American Journal of Physiology-Legacy Content*, 148(2):372–375.

Baumann, S. B., Wozny, D. R., Kelly, S. K., and Meno, F. M. (1997). The electrical conductivity of human cerebrospinal fluid at body temperature. *IEEE transactions on biomedical engineering*, 44(3):220–223.

Brindley, G. (1955). The site of electrical excitation of the human eye. *The Journal of physiology*, 127(1):189.

Brindley, G. (1956). The passive electrical properties of the frog's retina, choroid and sclera for radial fields and currents. *The Journal of physiology*, 134(2):339–352.

Dimbylow, P. (2011). Spherical polar co-ordinate calculations of induced fields in the retina and head for applied magnetic fields at 50 hz. *Physics in Medicine & Biology*, 56(14):4597.

Evans, I. D., Palmisano, S., and Croft, R. J. (2021). Retinal and cortical contributions to phosphenes during transcranial electrical current stimulation. *Bioelectromagnetics*, 42(2):146–158.

Evans, I. D., Palmisano, S., Loughran, S. P., Legros, A., and Croft, R. J. (2019). Frequency-dependent and montage-based differences in phosphene perception thresholds via transcranial alternating current stimulation. *Bioelectromagnetics*, 40(6):365–374.

Gabriel, C., Gabriel, S., and Corthout, y. E. (1996a). The dielectric properties of biological tissues: I. literature survey. *Physics in medicine & biology*, 41(11):2231.

Gabriel, C., Peyman, A., and Grant, E. H. (2009). Electrical conductivity of tissue at frequencies below 1 mhz. *Physics in medicine & biology*, 54(16):4863.

Gabriel, S., Lau, R., and Gabriel, C. (1996b). The dielectric properties of biological tissues: Iii. parametric models for the dielectric spectrum of tissues. *Physics in medicine & biology*, 41(11):2271.

ICNIRP (2010). Guidelines for limiting exposure to time-varying electric and magnetic fields (1 hz to 100 khz). *Health Physics*, 99(6):818–836.

ICNIRP (2020). Gaps in knowledge relevant to the "guidelines for limiting exposure to time-varying electric and magnetic fields (1 hz–100 khz)". *Health physics*, 118(5):533–542.

IEEE (2019). IEEE Standard for Safety Levels with Respect to Human Exposure to Electric, Magnetic, and Electromagnetic Fields, 0 hz to 300 GHz, IEEE Std C95.1-2019. *(New York: Institute of Electrical and Electronics Engineers)*.

Kanai, R., Chaieb, L., Antal, A., Walsh, V., and Paulus, W. (2008). Frequency-dependent electrical stimulation of the visual cortex. *Current Biology*, 18(23):1839–1843.

Kanai, R., Paulus, W., and Walsh, V. (2010). Transcranial alternating current stimulation (tacs) modulates cortical excitability as assessed by tms-induced phosphene thresholds. *Clinical Neurophysiology*, 121(9):1551–1554.

Kar, K. and Krekelberg, B. (2012). Transcranial electrical stimulation over visual cortex evokes phosphenes with a retinal origin. *Journal of Neurophysiology*, 108(8):2173–2178.

Laakso, I. and Hirata, A. (2012a). Computational analysis of thresholds for magnetophosphenes. *Physics in Medicine & Biology*, 57(19):6147.

Laakso, I. and Hirata, A. (2012b). Fast multigrid-based computation of the induced electric field for transcranial magnetic stimulation. *Physics in Medicine & Biology*, 57(23):7753.

Laakso, I. and Hirata, A. (2013). Computational analysis shows why transcranial alternating current stimulation induces retinal phosphenes. *Journal of neural engineering*, 10(4):046009.

Latikka, J., Kuurne, T., and Eskola, H. (2001). Conductivity of living intracranial tissues. *Physics in Medicine & Biology*, 46(6):1611.

Lindenblatt, G. and Silny, J. (2001). A model of the electrical volume conductor in the region of the eye in the elf range. *Physics in Medicine & Biology*, 46(11):3051.

Lövsund, P., Oberg, P., and Nilsson, S. (1979). Influence on vision of extremely low frequence electromagnetic fields. industrial measurements, magnetophosphene studies volunteers and intraretinal studies in animals. *Acta ophthalmologica*, 57(5):812–821.

Lövsund, P., Öberg, P., and Nilsson, S. (1980a). Magneto-and electrophosphenes: a comparative study. *Medical and Biological Engineering and Computing*, 18(6):758–764.

Lövsund, P., Öberg, P., Nilsson, S., and Reuter, T. (1980b). Magnetophosphenes: a quantitative analysis of thresholds. *Medical and Biological Engineering and Computing*, 18(3):326–334.

McCann, H., Pisano, G., and Beltrachini, L. (2019). Variation in reported human head tissue electrical conductivity values. *Brain topography*, 32(5):825–858.

Schutter, D. J. and Hortensius, R. (2010). Retinal origin of phosphenes to transcranial alternating current stimulation. *Clinical Neurophysiology*, 121(7):1080–1084.

Schwiedrzik, C. M. (2009). Retina or visual cortex? the site of phosphene induction by transcranial alternating current stimulation. *Frontiers in integrative neuroscience*, 3:6.

Soldati, M. and Laakso, I. (2020). Computational errors of the induced electric field in voxelized and tetrahedral anatomical head models exposed to spatially uniform and localized magnetic fields. *Physics in Medicine & Biology*, 65(1):015001.

Taki, M., Suzuki, Y., and Wake, K. (2003). Dosimetry considerations in the head and retina for extremely low frequency electric fields. *Radiation protection dosimetry*, 106(4):349–356.

Vurgese, S., Panda-Jonas, S., and Jonas, J. B. (2012). Scleral thickness in human eyes. *PLOS ONE*, 7(1):1–9.

Wang, W. and Eisenberg, S. R. (1994). A three-dimensional finite element method for computing magnetically induced currents in tissues. *IEEE Transactions on Magnetics*, 30(6):5015–5023.

Wood, A. W. (2008). Extremely low frequency (ELF) electric and magnetic field exposure limits: Rationale for basic restrictions used in the development of an australian standard. *Bioelectromagnetics*, 29(6):414–428.